The Opposition Effect of the Moon: The Contribution of Coherent Backscatter

Bruce W. Hapke,* Robert M. Nelson, William D. Smythe

The opposition effect, the sharp surge in brightness of an astronomical object observed near zero phase angle, which has been known for more than a century, has generally been explained by shadow hiding. The reflectances of several Apollo lunar soil samples have been measured as a function of phase angle in linearly and circularly polarized light. All samples exhibited a decrease in the linear polarization ratio and an increase in the circular polarization ratio in the opposition peak. This provides unequivocal proof that most of the lunar opposition effect is caused by coherent backscatter, not shadow hiding. This result has major implications for the interpretation of photometric observations of bodies in the solar system, including the Earth.

The surge in brightness of a particulate medium observed near zero phase angle (the angle between the directions to the source of illumination and the detector, as seen from the surface) is called the opposition effect (*1*) and has been known for over a century. It was first noted by Seeliger (*2*) on Saturn's rings and has since been observed on a variety of bodies, including the moon, Mars, asteroids, planetary satellites, and terrestrial materials, including vegetation (*3–5*). It appears to be a nearly ubiquitous property of objects in the solar system whose surfaces can be seen.

The explanation for the opposition effect that has been generally accepted during all this time is shadow hiding, in which particles in a planetary regolith cast shadows on adjacent particles; those shadows are visible at large phase angles, but, at zero phase, they are hidden by the particles that cast them. This model was first put forward by Seeliger (*2*) and, with subsequent modifications (*6*, *7*), has been a paradigm within the remote-sensing community. Because the width of the peak in the shadow-hiding model depends on the porosity and particle-size distribution (*7*), the model assumes great importance in efforts to infer physical properties of planetary regoliths from remote-sensing data.

Recently, another phenomenon that can cause an opposition effect has become widely known: coherent backscatter. This phenomenon, which is also known as weak photon localization and as time reversal symmetry, is based on the fact that portions of wave fronts that are multiply scattered within a nonuniform medium and follow the same path, but in opposite directions, combine constructively at zero phase angle to produce a brightness peak. The effect is most prominent when the particles are of the order of the wavelength in size and have high single-scattering albedos.

One of the earliest discussions of coherent backscatter was by Watson (*8*), who emphasized its importance in the interpretation of the backscattering of electromagnetic waves from plasmas. It was first invoked as an explanation for the opposition effect in the scattering of visible light from particulate media by Kuga and Ishimaru (*9*). Since then, a large number of experimental and theoretical papers on the topic have appeared in the literature (*10*). Models invoking coherent backscatter have had considerable success in explaining the unexpected radar properties of icy satellites (*11*).

It has been suggested that the opposition effects observed on bodies of the solar system at visual wavelengths might be caused by coherent backscatter (*11–13*). It has also been suggested (*13*, *14*) that the phenomenon can cause negative linear polarization and, hence, may account for the negative branch of polarization that has been observed on planetary bodies for over 60 years (*15*) but has never been adequately explained. Although these suggestions were plausible, they remained speculative because solar system objects are illuminated by natural sunlight, which is unpolarized, and observations that might be used (*11*) to decide the causes of the astronomical opposition effects either are not possible or have ambiguous interpretations.

There are several reasons why the hypothesis that coherent backscatter is the cause of the astronomical opposition effect has not been widely accepted. (i) Shadow hiding is a plausible physical mechanism that must occur in media in which the particles are much larger than the wavelength. (ii) The median size of lunar soil particles is about 40 μm (*16*), and it was not certain that there were sufficient numbers of small particles in the lunar regolith to allow appreciable coherent backscatter. (iii) The reflectances of many bodies of the solar system with strong opposition effects are low [the moon's Bond albedo, the fraction of incident light scattered in all directions, is about 7% (*17*)], and it was not clear whether there was sufficient multiply scattered light for coherent backscattering to be significant on their surfaces. (iv) The width of the lunar opposition effect is about 5°, whereas all of the coherent backscatter peaks from particulate media that had previously been studied in the laboratory had widths an order of magnitude smaller. (v) Both theory and experiment (*10*) predict that the width of the coherent backscatter peak is proportional to wavelength; however, no such dependence has been reported for the lunar opposition effect.

Specular reflection from a smooth surface preserves the direction of linear polarization but reverses the helicity of circular polarization. The polarization ratio of a medium is defined as the ratio of intensity scattered with the sense of polarization that would not be expected upon reflection from a smooth surface to the intensity scattered with the sense that would be expected. Hence, if linearly polarized light is incident, the linear polarization ratio is defined as $\mu_L = I_{LO}/I_{LS}$, where I_{LS} is the component of the radiance scattered with its electric vector in the same direction as that of the incident light and I_{LO} is the component scattered with its electric vector in the orthogonal sense. Similarly, if circularly polarized light is incident, the circular polarization ratio is defined as $\mu_C = I_{CS}/I_{CO}$, where I_{CS} is the radiance of the component scattered with the same helicity as the incident light and I_{CO} is that scattered with the opposite helicity.

A single scattering of light from a particle into the backward direction is mainly by specular reflection from the particle surface, which tends to preserve the direction of linear polarization but reverse the helicity of circular polarization. In general, multiple scatterings tend to randomize the polarization. However, many of the photons that contribute to the coherent backscatter have been scattered into the forward direction, which tends to preserve the original sense of linear polarization and original helicity of circular polarization (*10*). In shadow hiding, the opposition effect is caused entirely by singly scattered light; hence, μ_L and μ_C should both decrease as the phase angle approaches zero. By contrast, in coherent backscattering, the opposition effect involves only multiply scattered light; hence, because of the partial preservation of the original polarization state, μ_L should decrease, whereas μ_C should increase as the phase angle decreases within the opposition peak. It has also been suggested (*18*) that a high intensity in the backward direction might be caused by increased incoherent

B. W. Hapke, Department of Geology and Planetary Science, University of Pittsburgh, Pittsburgh, PA 15260.
R. M. Nelson and W. D. Smythe, Jet Propulsion Laboratory, Pasadena, CA 91109.
*To whom correspondence should be addressed.

multiple scattering. In that case, both μ_L and μ_C should increase in the opposition peak. Thus, measurement of both the linear and circular polarization ratios provides an empirical test for the determination of which phenomenon is the primary cause of the opposition effect in a given medium.

To carry out such a test, we obtained samples of lunar soil brought to Earth by the Apollo missions and measured their reflectances in light of linear and circular polarization (Table 1). Our measurements were done at two wavelengths with the use of a He-Ne laser at 633 nm (red) and a Cd laser at 442 nm (blue) as sources. The samples were illuminated at an angle of 5° from the vertical, and the intensity of light scattered from them measured in the principal plane on the same side of the vertical as the direction of illumination. During the measurements, the samples were continuously rotated on a turntable about a vertical axis to randomize effects of medium variability. By means of polarizing filters, the incident radiation was linearly polarized in a direction either parallel or perpendicular to the scattering plane, and the radiances scattered with polarization vectors parallel and perpendicular were measured. When quarter wave plates were added, right- or left-handed circularly polarized light was incident on the surface and measured at the detector.

Most of the samples were measured at phase angles between 1° and 70°; however, in circularly polarized red light, the samples were measured between 1° and 20°. Unfortunately, our apparatus prevented us from measuring the polarized reflectances at phase angles smaller than 1°; thus, we are not able to see the highest part of the opposition peak. However, this does not affect our conclusions. Also, the blue laser was less stable than the red one, so its data are somewhat more noisy.

We measured bidirectional reflectance as a function of the phase angle g (Fig. 1). The sharp increase in reflectances at angles smaller than about 5° is evident. For all samples, when g is larger than about 5°, both μ_L (Fig. 2) and μ_C (Fig. 3) increase as g increases. This is a result of the translucency of the particles, which increases the contribution of multiply scattered radiance at larger phase angles. However, as g decreases into the opposition peak, μ_L decreases, whereas μ_C increases. These results provide unequivocal evidence that most, if not all, of the opposition effect in each of the lunar samples is caused by coherent backscatter. For the brightest samples, the decrease in μ_L is minor, whereas $\mu_C > 1$, as predicted theoretically (*10, 11*).

The width of the coherent backscatter peak is given by $\Delta g \simeq \lambda/2\pi D$, where D is the transport mean free path for photons in the medium (*10*). For strongly absorbing particles like the lunar regolith, D is roughly the same as the spacing between scatterers. Because $\Delta g \simeq 0.1$, the scatterers responsible for the opposition effect apparently were separated by distances of the order of 1 μm. Because the mean particle size in the lunar regolith is around 40 μm (*16*), it is likely that these scatterers are small asperities on the surfaces of larger grains. This conclusion is consistent with experimental (*19*) and theoretical (*13*) studies, which show that wavelength-sized roughness on a surface can cause coherent backscatter. The width of the peak does not depend noticeably on wavelength; this can be explained if the scatterers responsible for the coherent backscatter have a wide size distribution (*20*).

The surfaces of most airless bodies in the solar system are heavily cratered, which implies the existence of lunar-like impact-generated regoliths on these bodies. The surprising observation that even the darkest lunar samples exhibit a pronounced increase in μ_C at small phase angles implies that coherent backscatter, rather than shadow hiding, is the primary cause of the opposition effects on all of these bodies. The very narrow opposition peaks on some

Table 1. Lunar samples and their normal albedo.

Sample number	Normal albedo	
	Blue (λ = 442 nm)	Red (λ = 633 nm)
10084	0.058	0.077
15041	0.065	0.094
15271	0.093	0.128
15601	0.076	0.102
61221	0.323	0.375
65701	0.116	0.153
75121	0.064	0.083
79221	0.063	0.084

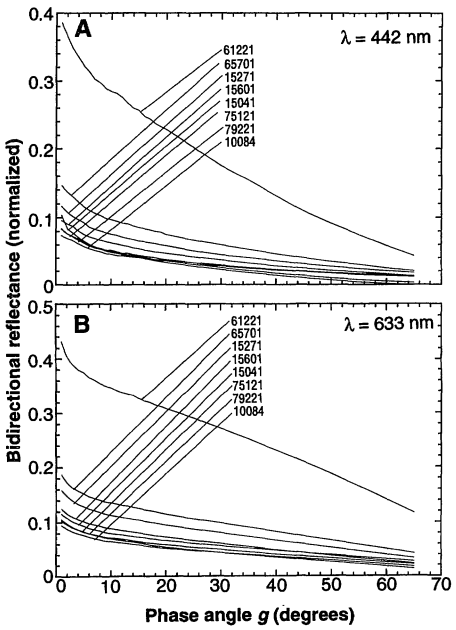

Fig. 1. Bidirectional reflectances of the lunar samples as a function of phase angle g in (**A**) blue light and (**B**) red light, normalized to their normal albedos, which are brightnesses relative to a halon standard at an incidence angle of 5°, viewing angle of 10°, and phase angle of 5° (Table 1).

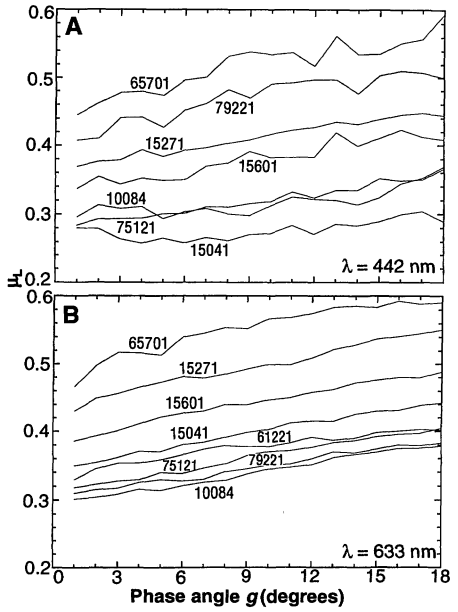

Fig. 2. Linear polarization ratio μ_L versus phase angle g in (**A**) blue light and (**B**) red light. The electric vector of the incident irradiance is perpendicular to the scattering plane (*21*).

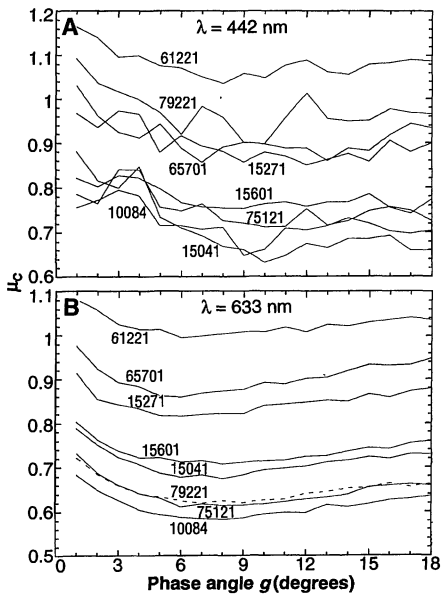

Fig. 3. Circular polarization ratio μ_C versus phase angle g in (**A**) blue light and (**B**) red light. The helicity of the incident irradiance is left-handed (*21*).

icy satellites (*4*) had severely strained the shadow-hiding models (*6*, *7*) but are easily explained by coherent backscatter. This phenomenon also accounts for the enhanced brightnesses of lunar rays near full moon, which shadow-hiding models have difficulty explaining.

These results also have implications for terrestrial remote sensing from aircraft and Earth orbiters. Like soil, vegetation exhibits an opposition effect, which is known to agronomists as the hot spot. Because of the large sizes and separations of leaves in vegetation compared with the wavelength, it is likely that most of the hot spot is caused by shadow hiding. However, individual leaves also exhibit an opposition peak (*5*), which may be caused by coherent backscatter between cells and other microscopic elements of the leaves. Which effect dominates the hot spot in vegetation remains to be determined.

Because shadow hiding must also occur in planetary regoliths, it is unlikely that coherent backscatter is the only cause of opposition effects. However, it appears that coherent backscatter dominates most of the opposition peaks observed in the solar system.

REFERENCES AND NOTES

1. T. Gehrels, *Astrophys. J.* **123**, 331 (1956). In this paper, Gehrels introduced the term "opposition effect."
2. H. Seeliger, *Abh. Bayer. Akad. Wiss. Math. Naturwiss. Kl. Sitzungsber.* **16**, 405 (1887); **18**, 1 (1895). Seeliger analyzed observations by G. Muller [*Publ. Astrophys. Obs. Potsdam No. 30* **8**, 193 (1893)].
3. T. Gehrels *et al.*, *Astron. J.* **69**, 826 (1964); P. Oetking, *J. Geophys. Res.* **71**, 2505 (1966); E. Whitaker, in "Analysis of Apollo 8 Photography and Visual Observations," *NASA SP-201*, 38 (1969); W. Egan and T. Hilgeman, *Appl. Opt.* **15**, 1845 (1976); T. Thorpe, *Icarus* **36**, 204 (1978); R. L. Wildey, *Science* **200**, 1265 (1978); W. Montgomery and R. Kohl, *Opt. Lett.* **5**, 546 (1980); A. Harris *et al.*, *Icarus* **81**, 365 (1989).
4. R. Brown and D. Cruikshank, *Icarus* **55**, 83 (1983); D. Domingue *et al.*, *ibid.* **90**, 30 (1991); D. T. Thompson and G. W. Lockwood, *J. Geophys. Res.* **97**, 14761 (1992).
5. P. Woessner and B. Hapke, *Remote Sensing Environ.* **21**, 243 (1987).
6. B. Hapke, *J. Geophys. Res.* **68**, 4571 (1963); W. Irvine, *ibid.* **71**, 2931 (1966); K. Lumme and E. Bowell, *Astron. J.* **86**, 1694 (1981).
7. B. Hapke, *Icarus* **67**, 264 (1986).
8. K. Watson, *J. Math. Phys.* **10**, 688 (1969).
9. Y. Kuga and A. Ishimaru, *J. Opt. Soc. Am. A* **1**, 831 (1984).
10. P. Wolf and G. Maret, *Phys. Rev. Lett.* **55**, 2696 (1985); F. MacKintosh and S. John, *Phys. Rev. B* **37**, 1884 (1988); K. Peters, *ibid.* **46**, 801 (1992); for a recent review, see A. McGurn, *Surf. Sci. Rep.* **10**, 357 (1990).
11. B. Hapke, *Icarus* **88**, 407 (1990); _____ and D. Blewett, *Nature* **352**, 46 (1991).
12. Y. Shkuratov, *Kinematics Phys. Celestial Bodies* **4**, 33 (1988); M. Mishchenko and J. Dlugach, *Mon. Not. R. Astron. Soc.* **254**, 15 (1992).
13. K. Muinonen, thesis, University of Helsinki (1990).
14. Y. Shkuratov, *Sol. Syst. Res.* **23**, 111 (1989).
15. B. Lyot, *Ann. Obs. Paris* **VIII**, 1 (1929).
16. D. McKay *et al.*, in *Proceedings of the Fifth Lunar Science Conference*, W. A. Gose, Ed. (Pergamon, New York, 1974), pp. 887–906.
17. D. Harris, in *Planets and Satellites*, G. Kuiper and B. Middlehurst, Eds. (Univ. of Chicago Press, Chicago, 1961), pp. 272–342.
18. S. Ostro and E. Shoemaker, *Icarus* **85**, 335 (1990).
19. K. O'Donnell and E. Mendez, *J. Opt. Soc. Am. A* **4**, 1194 (1987).
20. M. Mishchenko, *Astrophys. Space Sci.* **194**, 327 (1992).
21. For clarity, data for only one state of incident polarization are shown; curves for orthogonal states are almost identical.

22. We acknowledge the contributions of V. Gharakanian, L. Horn, and P. Hererra to the measurements reported here. This research was supported by grants from the Planetary Geology and Geophysics Program, Office of Space Science and Applications, National Aeronautics and Space Administration.

2 November 1992; accepted 4 March 1993

Manganese Oxide Octahedral Molecular Sieves: Preparation, Characterization, and Applications

Y. F. Shen, R. P. Zerger, R. N. DeGuzman, S. L. Suib,* L. McCurdy, D. I. Potter, C. L. O'Young*

A thermally stable 3 × 3 octahedral molecular sieve corresponding to natural todorokite (OMS-1) has been synthesized by autoclaving layer-structure manganese oxides, which are prepared by reactions of MnO_4^- and Mn^{2+} under markedly alkaline conditions. The nature and thermal stability of products depend strongly on preparation parameters, such as the MnO_4^-/Mn^{2+} ratio, pH, aging, and autoclave conditions. The purest and the most thermally stable todorokite is obtained at a ratio of 0.30 to 0.40. Autoclave treatments at about 150° to 180°C for more than 2 days yield OMS-1, which is as thermally stable (500°C) as natural todorokite minerals. Adsorption data give a tunnel size of 6.9 angstroms and an increase of cyclohexane or carbon tetrachloride uptake with dehydration temperature up to 500°C. At 600°C, the tunnel structure collapses. Both Lewis and Brönsted acid sites have been observed in OMS-1. Particular applications of these materials include adsorption, electrochemical sensors, and oxidation catalysis.

There are several naturally occurring manganese oxides with one-dimensional tunnel structures, such as hollandite, which consists of MnO_6 octahedra shared by vertices and edges making (2 × 2) octahedral unit tunnels (*1–3*), romanechite with (2 × 3) tunnels (*3*, *4*), todorokite with (3 × 3) tunnels, and materials with larger tunnels like (3 × 4) and (3 × 5) (*5–14*). Todorokite appears to be the most interesting of these because it has the largest tunnel (6.9 Å) as well as cation-exchange behavior like zeolites (*5*, *11*).

Natural todorokite is poorly crystalline, impure in composition, and coexists with other manganese oxide minerals. Applications of natural todorokite have therefore been limited, and the exact identification of this material is complicated. Many fundamental questions remain concerning the chemistry of todorokite.

Manganese oxides with hollandite tunnel structures (2 × 2) have been synthesized (*15*, *16*). A large crystal of $Rb_{0.27}MnO_2$ with a 2 × 5 structure has been prepared by reaction of β-MnO_2 with RbOH in a gold capsule at 350°C and 200 MPa (*17*). Todorokite was reported to be synthesized in 1971 (*18*), but its validity was doubted (*19*). Recently, Golden *et al.* reported the hydrothermal transformation of buserite (which has a layered structure) into todorokite (*20*, *21*). Initially the layered mineral birnessite forms and is ion-exchanged to form Mg birnessite (that is, buserite). However, no thermal stability was reported for their synthetic todorokite. We used the method of Golden *et al.* (*20*, *21*) to prepare todorokite, but the structure for the resultant material was found by x-ray diffraction (XRD) and surface area measurements [Brunauer-Emmett-Teller (BET) isotherms] to collapse on calcination at 300°C after 1 hour in contrast to natural todorokites, which are stable to at least 500°C (*22*).

Hydrothermal syntheses of the polymorphs of MnO_2 from reactions of MnO_4^- and Mn^{2+} are known to depend critically on the nature of precursors (*23*) and experimental conditions (*15*, *24*). We have developed $Mg(MnO_4)_2$-$MnCl_2$ reactions for preparing stable synthetic todorokite.

Washed Mg^{2+} layered manganese oxides, which were obtained by ion exchanging Na^+-type layered manganese oxides (*25*), were autoclaved at 155° to 170°C for 10 to

Y. F. Shen, R. P. Zerger, R. N. DeGuzman, Department of Chemistry, U-60, University of Connecticut, Storrs, CT 06269.
S. L. Suib, Departments of Chemistry and Chemical Engineering and Institute of Materials Science, U-60, University of Connecticut, Storrs, CT 06269.
L. McCurdy and D. I. Potter, Department of Metallurgy and Institute of Materials Science, University of Connecticut, Storrs, CT 06269.
C. L. O'Young, Texaco Research Center, Texaco, Inc., P.O. Box 509, Beacon, NY 12508.

*To whom correspondence should be addressed.